Latest advances and comparative analysis of MXenes as anode and cathode electrodes in secondary batteries

Konstantina A. Papadopoulou,[1,2] Alexander Chroneos,[3,4] and Stavros-Richard G. Christopoulos[5,6,*]

[1]*Department of Physics and Astronomy, Faculty of Environment, Science and Economy, University of Exeter, EX4 4QL, Exeter, UK*
[2]*Faculty of Engineering, Environment and Computing, Coventry University, Priory Street, Coventry, CV1 5FB, United Kingdom*
[3]*Department of Electrical and Computer Engineering, University of Thessaly, 38221 Volos, Greece*
[4]*Department of Materials, Imperial College London, London SW7 2BP, UK*
[5]*Department of Computer Science, School of Computing and Engineering, University of Huddersfield, HD4 6DJ, Huddersfield, UK*
[6]*Centre for Computational Science and Mathematical Modelling, Coventry University, Coventry CV1 2TU, UK*

MXenes, the two-dimensional derivative of the MAX phases, have attracted the interest of the community due to their unique materials properties. The field of MXenes for energy storage applications has expanded significantly in the past few years and in particular since the beginning of 2021. In the present comprehensive review we focus on the advances over the past two years in the use of MXenes for anodes and cathodes in batteries. We consider both experimental and theoretical studies and, as design criteria focus mainly on the surface migration energy barrier, the specific capacity and the rate capability.
Keywords: MXenes, Diffusion barrier, rechargeable batteries

I. INTRODUCTION

MXenes are a type of ceramic material that count a decade of life, firstly discovered in 2011 at Drexel University[1]. With their general formula being $M_{n+1}X_nT_x$, *(n=1,2,3)*, where T is a surface termination atom, M is an early transition metal, and X is either C or N[2–4], MXenes are directly etched from their corresponding MAX phases. The latter are layered carbide or nitride structures, with the formula $M_{n+1}AX_n$, *(n=1,2,3)*, where now A is an element from the A-group of the periodic table, usually groups 13 or 14. In Fig. 1 we can see the components of the MAX phases and MXenes in the periodic table, alongside their structures.

The titanium carbide Ti_3C_2 with OH or F terminaitons was the first MXene discovered from the titanium-aluminum MAX phase Ti_3AlC_2[1]. Owing to the fact that the $Ti_3C_2T_x$ MXene remains the most conductive one[6–8], it has been examined extensively in literature regarding its potential to be used in secondary, i.e., rechargeable, batteries. To that end, control of its electronic and mechanical properties is sought, by manipulating the termination atoms[8,9].

Rechargeable ion batteries are energy storage devices whose operation is based on the intercalation of ions[10]. In general, an ion battery consists of a cathode (positive electrode) and an anode (negative electrode) in contact with an electrolyte which contains ions. The two electrodes are separated by a microporous polymer membrane (separator) which stops the electrons from passing between them alongside the ions[11].

Commercial battery cells are usually produced in a discharged state, while the anode and cathode electrodes need to be stable when in contact with the atmospheric air[11]. For charging, the electrodes need to be connected to an external electrical power supply while the battery is enclosed in a closed circuit[10].

During charging of an ion battery cell, ions leave the positive electrode and move through the electrolyte to the negative electrode. We have, therefore, a storage of energy to the anode. During discharging of the battery, this energy is released, powering the battery, and the ions move back to the cathode. This process is called redox (reduction - oxidation) reaction as the anode gets oxidized and releases electrons to the external circuit while the cathode gets reduced (in charge) by accepting the electrons.

In more detail, electrons are forced to be released at the cathode and move to the anode through the external circuit during charging. At the same time, the ions move internally in the same direction via the electrolyte. The opposite happens during discharging[11]. Essentially, an ion battery converts chemical energy to electrical energy. The latter is extracted at a certain voltage[12].

One of the most active research fields regarding secondary batteries is the increase of their rate performance in order to reduce charging time which is important to the electric vehicles' market[13]. The materials of the electrodes are crucial for the performance of the battery, as they determine capacity, cell voltage and cyclability[11].

Regarding the cathodes, high voltage is required because the stored energy is proportional to the operating voltage of the cell[11]. One should be careful, however, when selecting cathode materials, as the high voltage can potentially affect the electrolyte's stability, causing decomposition and decreasing the life span of the battery cell.

When it comes to ion batteries, we need electrode materials that allow for high ion mobility. When the ion has the ability to move easily inside or on the surface of the material, the battery can achieve fast charge/discharge rates, a property that is significant for the enhanced op-

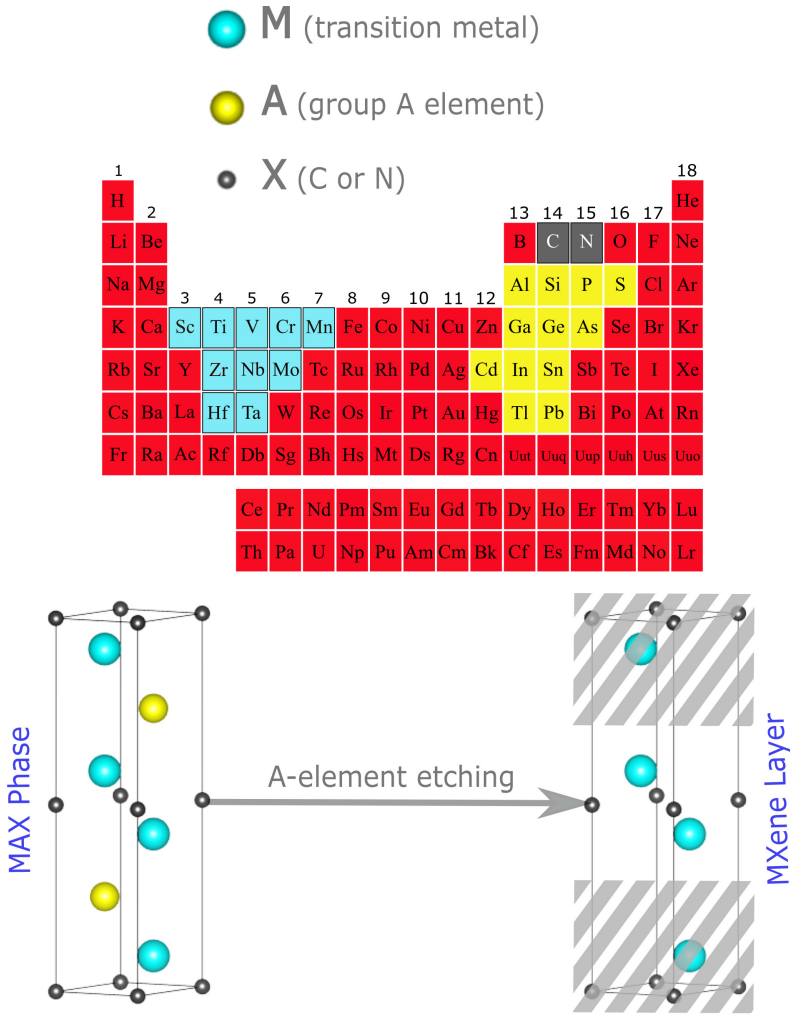

FIG. 1: The primitive cell of a M_2AX MAX-phase[5] (bottom left panel), alongside the primitive cell of the resulted M_2X MXene[5] (bottom right panel). The blue spheres represent the M atoms, the yellow the A atoms, and the black the X (here C) atoms. The top panel indicates the location, in the periodic table, of the components of a MAX phase.

eration of the battery since it determines the available stored energy. For example, expressing the battery's discharge current as a C-rate (measure of discharge rate relative to the maximum capacity)[14], a battery with a capacity of 2.3 Ah being discharged at a C-rating of 1C means that it can provide 2.3 A current for one hour. However, if we increase the discharge rate to 2C, the battery will last for half that time, i.e., 30 minutes, but it will provide double the current, i.e., 4.6 A. This is important for applications that require a powerful energy burst in a short time, like jump starting a vehicle, robotics and drones. Therefore, it is important not only to have batteries that can charge fast, but, in some cases, also discharge fast, and both of these properties can be controlled by the ion mobility.

The measure of the mobility of the ion is the energy barrier for diffusion (or activation energy), i.e., the minimum amount of energy the ion requires in order to break the bonds with its surrounding atoms and start moving (migrating) inside or on the surface of the material. For high mobility, we require low activation energy, since reactions that have lower activation energy happen more quickly. It is imperative, therefore, for the enhanced operation of energy storage devices like batteries, to have materials where the ions have low activation energies.

Anode materials are still predominantly carbon-based. In Li-ion batteries in particular, layered graphite structures facilitate the mobility of the Li ions leading to very good cyclability[15]. In intercalation compounds like graphite, ions intercalate between the layers of the compound by increasing the distance between the layers. However, this kind of anodes have almost reached their theoretical maximum capacity ($372\,\mathrm{mAhg}^{-1}$[11]). Carbon alternatives are being sought, safer and having high energy density, in order to meet the increasing demand coming from electric vehicles[16]. Materials like Si/C[17],

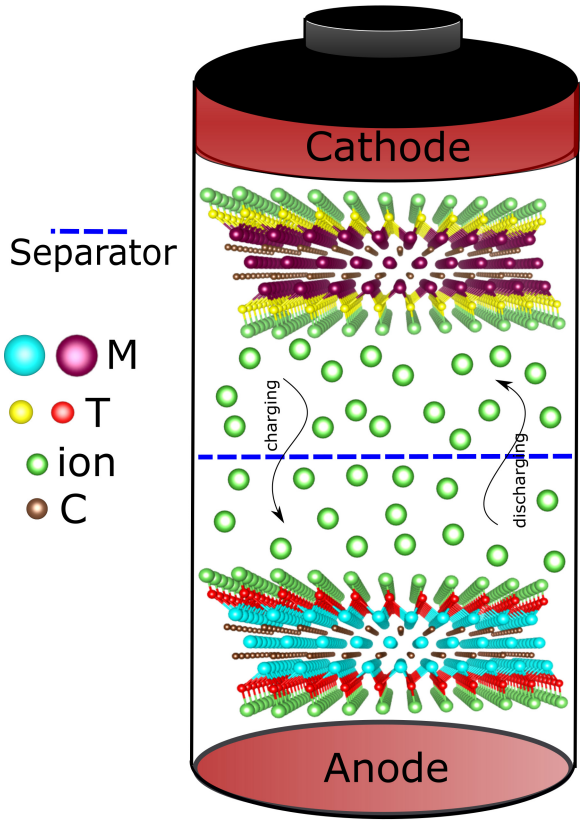

FIG. 2: A secondary battery with $M_3C_2T_x$ MXenes for anode and cathode electrodes.

SnO_2/C[18], metal oxides[19], TiO_2[20] and Si-based[11] materials have been extensively studied.

During the last two years, the field of MXenes as anode and cathode electrodes has exploded with experimental and theoretical studies. The main criteria used throughout the literature to determine an MXene's use as electrode is the energy barrier for diffusion of an ion on its surface, the material's specific capacity and the rate capability, i.e., the amount of capacity it can retain after a large number of cycles. In this paper, we present a comprehensive review regarding the use of MXenes in anode (Section II) and cathode (Section III) electrodes in literature for the years 2021-2022.

II. MXENES FOR ANODE ELECTRODES

In Figure 2 we can see the inner workings of a secondary battery, with MXenes as anode and cathode electrodes.

A. 2021

In 2021, Wang et al.[21] discussed how the interlayer distance in MXenes changes when the applied potential changes, thus changing an ion's resistance to movement during the battery's operation. Some ions, when intercalated in MXenes, can lead to shortening of the interlayer distance, making the ion transport more difficult. Wang et al. proposed that the preintercalation of ions into MXene structures can increase the interlayer distance and improve the ion transport, especially the preintercalation of larger ions like K.

In addition, Li et al.[22], using density functional theory calculations, examined the double-metal TiVC MXene, as well as the terminated $TiVCT_2$ (T = O, S, F, or OH) for anode electrodes in lithium-ion batteries. They found that, on the titanium surface of the pure TiVC, Li has a diffusion barrier as low as 15 meV, while on the vanadium surface the diffusion barrier is 14 meV. However, when the TiVC is terminated, the diffusion barrier increases, with $TiVCS_2$ exhibiting the lowest values (0.191 eV and 0.186 eV on the Ti and the V surfaces respectively).

Xia et al.[23] used the chemical vapor deposition method to synthesize nitrogen-doped graphene with $ReSe_2$ sandwiched between its layers, using the Ti_3C_2 MXene as substrate. They found that the material had improved structural stability, while, when it was used as anode electrode in potassium-ion batteries, it exhibited a reversible capacity of 90 $mAhg^{-1}$ at 5 Ag^{-1} after 300 cycles. Furthermore, Zhong et al.[24] synthesized MgH_2 nanoparticles and anchored them on a Ti_3C_2 MXene using a solvothermal technique. They found that the MXene can act as a substrate to improve the kinetics of Li ions while the constructed anode electrode had a reversible capacity as high as 1092.9 $mAhcm^{-3}$ at 2 Ag^{-1} after 1000 cycles.

Saha et al.[25] presented a novel experimental method to modify the surface of the $Ti_3C_2T_x$ MXene using atomic surface reduction. They synthesized a material with surface termination atoms rich in Al without changing the MXene's crystal structure and bulk properties. The resulting surface-modified $Ti_3C_2T_x$ MXene showed improved cycling stability and a capacity value equal to 58 $mAhg^{-1}$ while the pure MXene had 41 $mAhg^{-1}$.

Moreover, Papadopoulou et al.[26], used computational methods to study the $Ti_3C_2T_x$ MXene (T = O, S, Se, F, Cl, Br) as anode electrode in Li-ion batteries. They found that $Ti_3C_2Cl_2$ has a very low diffusion barrier for the Li ion, equal to 0.03 eV, a value that is significantly lower than all the others reported in literature so far using the $Ti_3C_2T_x$ MXene as the basis material.

Cheng et al.[27] examined the Nb_2CT_x MXene regarding its use as anode electrode. Through both experimental and computational methods, they found that when the O terminations are dominant, the MXene stores charge due to changes in the oxidation states of both Nb and O. Finally, when the Nb_2CT_x was combined with a $LiFePO_4/C$ cathode, the battery cell exhibited higher rate capability and cycling stability.

Also in 2021, Rajput et al.[28] studied the Ca_2C MXene as negative electrode in metal-ion batteries using first-principle calculations. They found very low energy barriers for ion migration, i.e., 0.027 eV, 0.059 eV, and 0.028 eV, for lithium, sodium, and potassium ions

respectively, indicating high ion mobility, thus fast charge/disharge rates. Furthermore, Maughan et al.[29] synthesized a porous Mo_2TiC_2 MXene and examined its use in lithium- and sodium-ion batteries. They found that the material retained 80% of its initial capacity even after 500 cycles while it also had superior capacity when compared to the non-porous Mo_2TiC_2 MXene.

Zhao et al.[30] doped the $Ti_3C_2T_x$ MXene (T = O or OH) with Fe and, via means of density functional theory calculations, found that the electron transfer in the Fe-O bond leads to unsaturated O atoms which in turn improve the lithium ion's adsorption. In addition, Ma et al.[31] designed a bismuth (Bi)-based anode material with the $Ti_3C_2T_x$ MXene as substrate. The electrode exhibited rapid ion transport and could maintain its specific capacity for 2500 cycles. Using this Bi/MXene for anode, the authors found that the battery cell could complete a full charge/discharge cycle in seven minutes.

Wang et al.[32], on the other hand, synthesized an N-doped, C-decorated $TiO_2/Ti_3C_2T_x$ MXene using polyethyleneimine. The resulted MXene, due to its own high conductivity and titanium-oxide's high capacity, had a very good performance, maintaining its capacity after 1900 cycles in sodium-ion batteries.

Also regarding sodium-ion batteries, Gou et al.[33] studied the Ti_3C_2 MXene with silicon nanoparticles which were coated with hard carbon and uniformly distributed on its surface. The authors found that portholes for fast sodium ion transport were created in the material, thus achieving fast Na^+ conduction. In addition, Liang et al.[34] synthesized the $Ti_2C_{0.5}N_{0.5}T_x$ carbonitride MXene and examined its performance in sodium-ion batteries. They found that the multilayered $Ti_2C_{0.5}N_{0.5}T_x$ powder has the highest specific capacity from all MXene electrodes reported so far in sodium-ion batteries.

Wang et al.[35] proposed a vanadium oxide-based $NHVO/Ti_3C_2T_x$ anode for Zn-ion batteries. The constructed material had high capacity ($514.7\,mAhg^{-1}$ at $0.1\,Ag^{-1}$), retaining it by 84.2% at $5\,Ag^{-1}$ after 6000 cycles.

Dong et al.[36] investigated the VN_2 MXene as anode electrode in lithium, sodium and potassium ion batteries using density functional theory calculations. The found very low ion migration barriers, i.e., 201.1 meV for Li, 84.1 meV for Na and 34.7 meV for K indicating very good rate performances. In addition, the largest calculated open-circuit voltage was 0.81 V for Li, a fact that further supports the promise of VN_2 as anode electrode.

Also using a vanadium-based MXene, Dinda and Meena[37] studied the V_3C_2 MXene/graphene heterostructure as electrode in metal ion batteries using a computational design. They found low energy barriers for diffusion, namely 0.11 eV for a Li ion, 0.17 eV for a Na ion and 0.15 eV for a Ca ion. This fact indicated fast charge/discharge rates, thus rendering the MXene/graphene heterostructure a suitable material for anode electrode.

Chen et al.[38] hydrothermally synthesized an SnO_2/MXene composite and examined its use as anode in sodium-ion batteries. The MXene they used as substrate was once again the $Ti_3C_2T_x$ and the dispersion of SnO_2 on the MXene's surface improved the charge transfer and Na^+ transfer. Furthermore, Zhu et al.[39] also synthesized an SnO_2-Ti_2C composite anode coated with graphite nanosheets. The added carbon in the coating prevented SnO_2 from turning into powder, while the SnO_2 nanoparticles shortened the Li ion's diffusion pathways.

Moreover, Dong et al.[40] synthesized the Nb_2CT_x MXene by means of Lewis acidic etching. They found that the prepared material had maximum Li ion storage capacity up to $330\,mAhg^{-1}$ at $0.05\,Ag^{-1}$, outperforming the $Ti_3C_2T_x$ MXene by 61%. In addition, Wang et al.[41] synthesized a sodium/reduced graphene oxide/MXene (Na@rGO/MXene) anode electrode for use in sodium-metal batteries. The MXene used was the $Ti_3C_2T_x$ and the symmetric cell showed high cycling stability even after 1700 h. Furthermore, Chen et al.[42] synthesized a W-doped $Nb_2O_5/Ti_3C_2T_x$ nanocomposite to use as negative electrode in Li-ion batteries. They found that the addition of the MXene was a main factor to the improvement of the electrochemical performance of Nb_2O_5, with the material retaining the 96.3% of its capacity after 500 cycles.

Tian et al.[43] grew Sb nanoarrays on a $Ti_3C_2T_x$ MXene paper and examined the fabricated material as anode electrode in Zn-based batteries. They found that Sb alloyed with Zn, thus reducing the risk of Zn dendrites formation, while the battery had a cycling life reaching 1000 h. In addition, Fan et al.[44], designed an anode electrode consisting of Sn_4P_3 nanoparticles sandwiched between layers of the $Ti_3C_2T_x$ MXene. While the phosphides in general have poor structural stability, the authors found that the addition of the MXene allows the large volume change of Sn_4P_3 during lithiation without breakage. In addition, the material had a high specific capacity of $820\,mAhg^{-1}$ at $1\,Ag^{-1}$ after 300 cycles.

Finally, Guo et al.[45], in order to overcome the slow kinetics of Li ions in Fe_3O_4, they wrapped Fe_3O_4 nanospheres with Ti_3C_2 MXene and then embedded them in nitrogen-doped carbon nanofibers (Fe_3O_4@Ti_3C_2/CNFs). When used as anode in Li-ion batteries, density functional theory calculations showed that the adsorption of Li ions was significantly enhanced with a specific capacity of $806\,mAhg^{-1}$ at $2\,Ag^{-1}$ after 500 cycles.

B. 2022

In 2022, Zha et al.[46] studied theoretically the use of Ti- and Zr-based MXenes as anodes in sodium-ion batteries. They found that $Ti_3C_2O_2$ is the most promising candidate, with a migration barrier for the Na ion equal to 0.138 eV. In addition, they showed that $Zr_3C_2O_2$ and $Zr_3C_2S_2$ can adsorb two layers of Na atoms on both of

their sides, while the former exhibits higher capacity than the latter because it is lighter and has smaller volume.

Furthermore, Zhu et al.[47] developed a low-cost electrolyte to control the reaction kinetics of MXene electrodes. They used LiCl salt to fabricate the electrolyte and they found that, after placing the $Ti_3C_2T_x$ MXene into the LiCl electrolyte, the interlayer distance of the MXene was increased. This fact led to the prevention of MXene deterioration (oxidation) in high voltages.

Alli et al.[48] synthesized a nitrogen-doped Ti_2C MXene/TiO_2 hybrid for use as anode electrode in Li-ion batteries, following the Continuous Hydrothermal Flow Synthesis (CHFS) synthesis method which is aqueous-based. The electrode had a specific capacity of 369 $mAhg^{-1}$ after 100 cycles, outperforming the Ti_2C/C nanocomposites.

Papadopoulou et al.[49] theoretically studied the $Ti_3C_2S_2$ MXene as anode electrode in Mg-ion batteries. They found an energy barrier of 0.049 eV for the Mg ion, a fact that indicated fast charge/discharge rates for Mg-ion batteries with $Ti_3C_2S_2$ negative electrodes. In the same year, in a different study, Papadopoulou et al.[50] also studied the Li, K, Mg and Zn ion diffusion on the Zr_2CS_2 MXene. They found the following diffusion barriers, respectively: 0.25 eV, 0.10 eV, 0.15 eV, 0.19 eV. The authors proposed that K-ion batteries are a good alternative for Li-ion batteries as they also have higher energy density.

Also in 2022, Shi et al.[51] used computational methods to study the interface between antimony oxychloride ($Sb_4O_5Cl_2$) and the Ti_3C_2 MXene. They proposed that the hybrid $Sb_4O_5Cl_2$-Ti_3C_2 can be used as anode electrode in potassium-ion batteries since the Sb atoms optimize the migration pathway of the potassium ion, reducing its energy barrier for diffusion.

Moreover, Liu et al.[52] studied the V_2N MXene for anode electrode in ion batteries using first-principles calculations. They found that the K ion has a diffusion barrier almost zero (0.004 eV), the Na ion 0.014 eV, the Li ion 0.025 eV and the Mg ion 0.058 eV. In addition, they found for the Na, Li and Mg cases an open-circuit voltage lower than 1 eV, a fact that indicates that the V_2N MXene is feasible for ion batteries, with the best case being the sodium-ion ones.

Guo et al.[53] on the other hand, investigated the α-MoO_3/MXene composite as anode electrode for lithium storage devices. MoO_3 itself has poor conductivity, but adding an MXene substrate greatly improves its performance. The authors used the Ti_3C_2 MXene as substrate to fabricate a free-standing electrode and noted an improvement in lithium ion transport and a high lithium ion storage capacity at 1008 $mAhg^{-1}$ at 0.1 Ag^{-1}. Furthermore, Tariq et al.[54] experimentally studied the TiO_2-encrusted Ti_3C_2 MXene as anode electrode. TiO_2 also has low electrical conductivity on its own, but the presence of the MXene once again enhanced the electrode's performance. In particular, Tariq et al.[54] found an increase in SSA up to 379% from the Ti_3C_2 MXene without the added TiO_2, and a lower activation energy for the lithium ion.

Han et al.[55] designed a silicon/MXene anode electrode with interfacial nitrogen engineering using the $Ti_3C_2T_x$ MXene. During this process, they found that Si is shelled by amorphous carbon and that the silicon-nitrogen bond at the interface between silicon and amorphous carbon facilitates fast Li ion transport. Moreover, Wu et al.[56] used the $SnCl_2$ molten salt to synthesize the $Ti_3C_2T_x$ MXene from the Ti_3AlC_2 MAX phase. The resulted MXene had Sn nanoparticles confined between its layers. These nanoparticles increased the interlayer distances, thus improving the Li-ion storage.

Ma et al.[57] grew *in-situ* Nb-doped TiO_2 nanosheets on the double transition metal $TiNbCT_x$ MXene. The material they synthesized had high conductivity and structure stability, while the large layer interspace created improved the kinetics of the Li ion. Furthermore, Wu et al.[58] wrapped porous $TiNb_2O_7$ spheres with $Ti_3C_2T_x$ MXene and examined it as anode in both liquid and solid state Li-ion batteries. They found that the presence of the MXene enhanced $TiNb_2O_7$'s electronic conductivity by four orders of magnitude while oxygen vacancies improved the Li ion transport.

Wang et al.[59] used first-principles calculations to study the V_2CSe_2 MXene for anode electrode in sodium- and calcium-ion batteries. They found a very low diffusion barrier for the Na ion equal to 0.098 eV, while for the Ca ion the diffusion barrier was greater and equal to 0.24 eV. In both cases, the open-circuit voltage did not exceed the 0.2 V, constituting the V_2CSe_2 monolayer a promising anode electrode. Moreover, Zhang et al.[60] synthesized the V_2CT_x MXene with Ag nanoparticles grafted on it. The V_2CT_x/Ag anode electrode with 4% Ag concentration had a Li specific capacity of 631 $mAhg^{-1}$ at 0.05 Ag^{-1}, falling to 298 $mAhg^{-1}$ at 5 Ag^{-1} after 2000 cycles, exhibiting, therefore, high rate capability.

Gong et al.[61], also using first-principles calculations, studied the Mn_2NO_2 MXene as anode electrode in Li^+-, Na^+-, K^+-, Mg^{2+}-, Ca^{2+}- and Al^{3+}-ion batteries. They found, for each case, the following energy barriers for diffusion respectively: 0.28 eV, 0.72 eV, 0.33 eV, 0.49 eV, 0.48 eV, 1.10 eV. These values are much higher than other MXenes and Mn_2NO_2 was found to have poor energy storage capacitance for lithium-, potassium- and calcium-ion batteries but it was more suitable for magnesium-ion batteries.

Qian et al.[62], designed an MXene-based Li metal anode with a solid electrolyte interphase (SEI). They used the Ti_3C_2 MXene and found that the constructed anode retained its capacity by 95.7% after 200 cycles (300 $mAhg^{-1}$). Moreover, Wei et al.[63] studied the Ti_2CT_2 MXene (T = F, O, OH) via first-principles calculations for use as anode electrode in Li-,Na-,Mg-, and Al-ion batteries. They found that best performance had the MXene with O terminations for Mg-ion batteries. In particular, Ti_2CO_2 had an Mg ion capacity of more than 1500 $mAhg^{-1}$.

Zhou et al.[64] created a $Ti_3C_2T_x$/graphene anode for

use in Zn-ion batteries. They found that the electrode had an initial capacity of $110\,mAhg^{-1}$ at $2\,Ag^{-1}$, retaining this value by 90.3% when using $LiMn_2O_4$ for cathode. Moreover, Yuan et al.[65] studied the S-terminated $Ti_3C_2T_x$ MXene as anode electrode in Li-ion batteries, both experimentally and computationally. They found that the material had a reversible capacity of $167.8\,mAhg^{-1}$ at $0.5\,Ag^{-1}$ after 100 cycles, and falling only to $166.3\,mAhg^{-1}$ at $0.5\,Ag^{-1}$ after 400 cycles.

Zhang et al.[66], in order to overcome the fact that MoS_2 expands in volume, they aligned it vertically on $Ti_3C_2T_x$ MXene nanosheets that had partially oxidised dual-phased TiO_2 (MoS_2@$Ti_3C_2T_x$@D-TiO_2). The material was the used as anode in sodium-ion batteries, and it was found to have a specific capacity of $359.6\,mAhg^{-1}$ for up to $5\,Ag^{-1}$ at room temperature. Furthermore, Seo et al.[67] fabricated hollow $Ti_3C_2T_x$/C nanofibers for use as anode electrodes in lithium-ion batteries. The authors found a specific capacity of $306.5\,mAhg^{-1}$ at $0.04\,Ag^{-1}$, significantly enhanced from the $81.08\,mAhg^{-1}$ of the MXene paste and the $196.9\,mAhg^{-1}$ of the MXene/carbon paste at the same current density.

Deng et al.[68] coupled Co - Ni selenide nanosheets with a Ti_3C_2 substrate for use as anode electrode in sodium-ion batteries. The electrode had an initial capacity of $337\,mAhg^{-1}$ at $3\,Ag^{-1}$ and $338\,mAhg^{-1}$ at $1\,Ag^{-1}$ after 600 cycles. In addition, He et al.[69] designed a hydroxylated Ti_3C_2 MXene (h-Ti_3C_2) with Stepped Sodiophilic Gradient structure (h-MXene-SSG) for anode in rechargeable Na-O_2 batteries. The material had a reversible capacity of $1000\,mAhg^{-1}$ at $1\,Ag^{-1}$. Meanwhile, Carvalho et al.[70] used the $Ti_1Al_1TiC_{1.85}$ MXene as anode electrode to compare the environmental impact of lithium-ion and sodium-ion batteries. They found that the lithium-based battery has better environmental performance, because the sodium one had lower energy density.

Ghaed et al.[71] studied the Ca_2C MXene as anode in Li-ion batteries using molecular dynamics and density functional theory methods. The electrode had a low open-circuit voltage (0.3 V) and its ionic conductivity increased with temperature. Moreover, Liu et al.[72] synthesized the C-intercalated Nb_2CT_x MXene (Nb_2CT_x/C) for use as anode in potassium-ion batteries. The electrode had an initial capacity of $397.9\,mAhg^{-1}$ at $0.02\,Ag^{-1}$ and $338.1\,mAhg^{-1}$ at $0.1\,Ag^{-1}$, maintaining it by 80% and 76.2% respectively after 100 cycles.

Qian et al.[73] constructed a Li-In-$Ti_3C_2T_x$ anode, using electrodeposition to fabricate In seeds on the MXene's surface. The material had specific Li capacity of $103.37\,mAhg^{-1}$ at $0.2\,Ag^{-1}$, falling to $82.74\,mAhg^{-1}$ at $0.2\,Ag^{-1}$ after 130 cycles. Therefore, the authors concluded that the indium seeds are lithiophilic and that they enable the construction of a stable anode.

Cui et al.[74] studied submicron Ti_2CT_x (s-Ti_2CT_x), i.e., MXene particulates less than a micron, which where synthesized using the molten salt method. When used as anode electrode in Li-ion batteries, the material had a specific capacity of $155\,mAhg^{-1}$ at $10\,Ag^{-1}$. Moreover, Zhao et al.[75] anchored SnO_2 nanosheets on the Ti_2CT_x MXene for use as anode electrode in Li-ion batteries. The SnO_2/Ti_2CT_x electrode had a specific capacity of $1550\,mAhg^{-1}$ at $0.1\,Ag^{-1}$ and a rate capability of $904\,mAhg^{-1}$ at $0.1\,Ag^{-1}$ after 1000 cycles. In comparison, the MXene had $220\,mAhg^{-1}$ while the SnO_2 had $200\,mAhg^{-1}$ capacity at the same current density.

Finally, Tian et al.[76] grew $Li_4Ti_5O_{12}$ nanoparticles on the Ti_2CT_x MXene for anode electrode in Li-ion batteries. The $Li_4Ti_5O_{12}$/Ti_2CT_x electrode had a specific capacity of $137\,mAhg^{-1}$ at $1.75\,Ag^{-1}$, retaining it by 87.5% after 1000 cycles.

In Table I we summarize the energy barriers for ion diffusion for all the anode materials mentioned above. It is evident that materials that include V as a transition metal show very fast ion kinetics, especially in the cases of nitride-based MXenes. Furthermore, Mn-based MXenes exhibit considerably higher ion diffusion barriers, a fact that renders them unsuitable for anode electrodes. In Table II we summarize the specific capacities and performance rates.

III. MXENES FOR CATHODE ELECTRODES

A. 2021

In 2021, Zhang et al.[77] synthesized a porous $Ti_3C_2T_x$ MXene decorated with $LiFePO_4$ and examined it as cathode electrode in Li-ion batteries. They found that the electrode retains the 94.8% of its capacity for 500 cycles, and that the MXene formed a conductive network, "bridging" the nanoplates and improving electron transfer.

Li et al.[78] examined the Nb_2CT_x MXene as cathode electrode in aqueous Zn-ion batteries. They found a high intrinsic voltage plateau at 1.55 V through repeated high-voltage scanning, which led to a high energy density of $146.7\,Whkg^{-1}$ with 63% contribution from the plateau. This fact signified the importance of the existence of a voltage plateau in the discharge curve. In the same year, Li et al.[79] fabricated the Ti_2C MXene with O and F termination atoms and examined its use as the positive electrode in Li-O_2 batteries. Using density functional theory calculations, they found that the O terminations enable a stable adsorption-nucleation-decomposition process for Li_2O_2 while the F terminations do not bond as strongly with Li_2O_2, thus reducing the catalytic capability of the material. In addition, Li et al.[80] examined the Nb_2CO_2 MXene as cathode in Li-O batteries. The synthesized electrode had a very large specific capacity of $19,785.5\,mAhg^{-1}$ at $0.2\,Ag^{-1}$ and was stable for 130 cycles $3\,Ag^{-1}$.

Zhao et al.[81], constructed a $Ti_3C_2T_x$ cathode for Li-S batteries. The latter have a large enough theoretical capacity ($1675\,mAhg^{-1}$) but poor cycling stability since the lithium polysulfide is highly soluble in organic elec-

TABLE I: Ion migration barriers in literature for the years 2021-2022 (alphabetically by material) for anode electrodes.

Material	Battery	Diffusion Barrier (eV)	Reference
Ca_2C	Li-ion	0.027	[28]
Ca_2C	Na-ion	0.059	[28]
Ca_2C	K-ion	0.028	[28]
Mn_2NO_2	Li-ion	0.280	[61]
Mn_2NO_2	Na-ion	0.720	[61]
Mn_2NO_2	K-ion	0.330	[61]
Mn_2NO_2	Mg-ion	0.490	[61]
Mn_2NO_2	Ca-ion	0.480	[61]
Mn_2NO_2	Al-ion	1.100	[61]
$Ti_3C_2Cl_2$	Li-ion	0.030	[26]
$Ti_3C_2F_2$	Li-ion	0.390	[26]
$Ti_3C_2O_2$	Li-ion	0.700	[26]
$Ti_3C_2O_2$	Na-ion	0.138	[46]
$Ti_3C_2S_2$	Li-ion	0.290	[26]
$Ti_3C_2S_2$	Mg-ion	0.049	[49]
TiVC (Ti surface)	Li-ion	0.015	[22]
TiVC (V surface)	Li-ion	0.014	[22]
$TiVCS_2$ (Ti surface)	Li-ion	0.191	[22]
$TiVCS_2$ (V surface)	Li-ion	0.186	[22]
V_3C_2/graphene	Li-ion	0.110	[37]
V_3C_2/graphene	Na-ion	0.170	[37]
V_3C_2/graphene	Ca-ion	0.150	[37]
V_2CSe_2	Na-ion	0.098	[59]
V_2CSe_2	Ca-ion	0.240	[59]
VN_2	Li-ion	0.201	[36]
VN_2	Na-ion	0.084	[36]
VN_2	K-ion	0.035	[36]
V_2N	K-ion	0.004	[52]
V_2N	Na-ion	0.014	[52]
V_2N	Li-ion	0.025	[52]
V_2N	Mg-ion	0.058	[52]
Zr_2CS_2	Li-ion	0.250	[50]
Zr_2CS_2	K-ion	0.100	[50]
Zr_2CS_2	Mg-ion	0.150	[50]
Zr_2CS_2	Zn-ion	0.190	[50]

trolytes. By encapsulating spheres of S in the $Ti_3C_2T_x$, the authors showed that the active mass loss was reduced while the material had a volumetric capacity of $2.7\,Ahcm^{-3}$ after 300 cycles. In addition, Wang et al.[82] synthesized a Co-$MoSe_2$/$Ti_3C_2T_x$ cathode also for Li-S batteries. The electrode had a specific capacity of $1454\,mAhg^{-1}$ at 0.1 C. Wei et al.[83], on the other hand, 3D printed a framework of N-doped porous $Ti_3C_2T_x$ (N-p$Ti_3C_2T_x$) for cathode electrode in Li-S batteries. The electrode exhibited the ability to immobilize the soluble polysulfide, thus making the electrode stabler, while it was versatile in that it could also be used as anode.

Furthermore, Zhang et al.[84] used the $Ti_3C_2T_x$ MXene with PDDA [Poly(diallyl dimethyl ammonium chloride)] as S-host in Li-S batteries. The PDDA/$Ti_3C_2T_x$ cathode, due to the use of the MXene, showed enhanced use of sulfur and, at the same time, prevented the polysulfides' shuttling. The initial specific capacity was $1016.8\,mAhg^{-1}$ at 0.2 C, with a very slow decay rate of 0.075% per cycle at 1 C. Here, 1 C=$1672\,mAg^{-1}$. Moreover, Yao et al.[85] used the nitrogen-based Ti_2NS_2 MXene as cathode in Li-S batteries. Using computational methods, they found that the electrode can inhibit the transfer of the highly soluble lithium polysulfides Li_2S_x more than the Ti_2NO_2 MXene, while density of states calculations showed that the material remains metallic, thus conductive.

Another study in Li-S batteries by Li et al.[86] utilized a graphene/$Ti_3C_2T_x$@S cathode constructed using the wet-spun method. The material had initial specific capacity of $1483.1\,mAhg^{-1}$ at 0.1 C, with 0.043% attenuation per cycle at 1 C for over 1000 cycles. Moreover, Xue et all.[87] embedded S nanoparticles in the $Ti_3C_2T_x$ MXene, using isopropyl alcohol (IPA) and CS_2 to dissolve S. The S/$Ti_3C_2T_x$-CS_2/IPA electrode was then used as cathode in a Li-S battery. It was found that the material had an initial specific capacity of $1474.5\,mAhg^{-1}$ at $0.1\,Ag^{-1}$, while it maintained $522.7\,mAhg^{-1}$ at $1\,Ag^{-1}$ for up to 1000 cycles.

Finally, Wang et al.[88] also designed an S-imbued $Ti_3C_2T_x$ for cathode in Li-S batteries, examining different sulfur concentrations. They found that the optimum S/$Ti_3C_2T_x$ electrode is the one with 67.0 wt% S content (4:1 mass ratio of sulfur to MXene), exhibiting $1277\,mAhg^{-1}$ initial capacity at 0.5 C and retaining $1059\,mAhg^{-1}$ of it after 100 cycles.

Also in 2021, Tan et al.[89] designed a MoS_2/$Ti_3C_2T_x$ MXene cathode electrode to enhance the performance of Al-ion batteries. They found that, while the pure MoS_2 cathode had a charge capacity up to $88.4\,mAhg^{-1}$ for 60 cycles, the MoS_2/$Ti_3C_2T_x$ composite had a charge capacity of $166\,mAhg^{-1}$ for the same amount of cycles. The presence of the MXene, therefore, vastly improved the electrochemical performance of the electrode. Finally, Tan et al.[89] also noted that the $Ti_3C_2T_x$ prevented the pulverization of MoS_2, thus resulting in a more stable structure.

Shi et al.[90], designed a VO_2/$Ti_3C_2T_x$ hybrid film for use as cathode electrode in Zn-ion batteries. They found that the presence of the MXene enhances the Zn ion's kinetics and the specific capacity ($228.5\,mAhg^{-1}$ at $0.2\,Ag^{-1}$) is retained by 72.1% after 2500 cycles. Also regarding Zn-ion batteries, Liu et al.[91] developed a composite of $Ti_3C_2T_x$ with $H_2V_3O_8$ nanowires grown on it. The $H_2V_3O_8$/$Ti_3C_2T_x$ cathode had $365.3\,mAhg^{-1}$ at $0.2\,Ag^{-1}$ specific capacity and a cycling stability lasting for 5600 cycles for $5\,Ag^{-1}$ current density. The authors indicate that these high values of capacity and stability could lead to a battery system that can sustain large-scale applications.

Using the V_2C MXene, Liu et al.[92] proposed it as a suitable cathode material in Zn-ion batteries. The authors found that, although the pristine material initially had a low specific capacity ($55\,mAhg^{-1}$), when charged at 1.8 V it changes to $423.5\,mAhg^{-1}$. However, for 2 V and above the specific capacity decreases again and this is contributed to the collapse of the MXene nanosheets.

TABLE II: Specific capacities and rate capabilities in literature for the years 2021-2022 (alphabetically by material) for anode electrodes.

Anode	Battery Type	Current Rate (Ag^{-1})	Initial Capacity ($mAhg^{-1}$)	Rate Capability	Durability (Cycles)	Reference
α-MoO_3/Ti_3C_2	Li-ion	0.1	1008	-	-	[53]
$Bi/Ti_3C_2T_x$	Na-ion	-	-	-	2500	[31]
$C@N/TiO_2/Ti_3C_2T_x$	Na-ion	-	-	-	1900	[32]
Co - $Ni/Se@Ti_3C_2$	Na-ion	3	337	$338\,mAhg^{-1}$ at $1\,Ag^{-1}$	600	[68]
$Fe_3O_4@Ti_3C_2/CNFs$	Li-ion	-	-	$806\,mAhg^{-1}$ at $2\,Ag^{-1}$	500	[45]
h-Ti_3C_2-SSG	$Na-O_2$	1	1000	-	-	[69]
hollow-$Ti_3C_2T_x/C$	Li-ion	0.04	306.5	-	-	[67]
$Li_4Ti_5O_{12}/Ti_2CT_x$	Li-ion	1.75	137	87.5%	1000	[76]
Li-In-$Ti_3C_2T_x$	Li-ion	0.2	103.37	$82.74\,mAhg^{-1}$ at $0.2\,Ag^{-1}$	130	[73]
$MoS_2@Ti_3C_2T_x@D$-TiO_2	Na-ion	5	359.6	-	-	[66]
Nb_2CT_x	Li-ion	0.05	330	-	-	[40]
Nb_2CT_x/C	K-ion	0.02	397.9	80%	100	[72]
Nb_2CT_x/C	K-ion	0.1	338.1	76.2%	100	[72]
$N/G/ReSe_2@Ti_3C_2$	K-ion	-	-	$90\,mAhg^{-1}$ at $5\,Ag^{-1}$	300	[23]
$N/Ti_2C/TiO_2$	Li-ion	-	-	$369\,mAhg^{-1}$	100	[48]
$NHVO/Ti_3C_2T_x$	Zn-ion	0.1	514.7	84.2% at $5\,Ag^{-1}$	6000	[35]
p-Mo_2TiC_2	Li-,Na-ion	-	-	80%	500	[29]
s-Ti_2CT_x	Li-ion	10	155	-	-	[74]
SEI-Ti_3C_2	Li-ion	-	-	95.7%	200	[62]
$Sn_4P_3/Ti_3C_2T_x$	Li-ion	-	-	$820\,mAhg^{-1}$ at $1\,Ag^{-1}$	300	[44]
SnO_2/Ti_2CT_x	Li-ion	0.1	1550	$904\,mAhg^{-1}$ at $0.1\,Ag^{-1}$	1000	[75]
Ti_2CO_2	Mg-ion	-	1500	-	-	[63]
$Ti_3C_2S_x$	Li-ion	-	-	$166.3\,mAhg^{-1}$ at $0.5\,Ag^{-1}$	400	[65]
$Ti_3C_2T_x$/graphene	Zn-ion	2	110	90.3%	-	[64]
V_2CT_x/Ag	Li-ion	0.05	631	$298\,mAhg^{-1}$ at $5\,Ag^{-1}$	2000	[60]
$W/Nb_2O_5/Ti_3C_2T_x$	Li-ion	-	-	96.3%	500	[42]

Moreover, Li et al.[93] synthesized a hybrid Zn-ion battery with V_2CT_x as cathode and $Ti_3C_2T_x$ as anode. The battery was stretchable, which made it suitable for wearable electronics, and it had a specific capacity of $118.5\,mAhg^{-1}$ at $0.05\,Ag^{-1}$ under 0% strain. This value remained high ($103.6\,mAhg^{-1}$) even after 50% strain.

Wang et al.[94] 3D printed a $V_2O_5/Ti_3C_2T_x$ nanosheet for use in Li-ion batteries. They found that the printed composite ink cathode had initial capacity equal to $321\,mAhg^{-1}$ at 1 C (1 C=$294\,mAg^{-1}$), retaining 91.8% of it after 680 cycles at 10.5 C.

Li et al.[95] synthesized the $Ti_3C_2T_x$ with halogen terminations, i.e., Cl, Br, I, ClBr, ClI, BrI, ClBrI, for use in Zn-ion batteries. At $0.5\,Ag^{-1}$ current density, the initial specific capacities were found equal to $46.5\,mAhg^{-1}$ for $Ti_3C_2Cl_2$, $97.6\,mAhg^{-1}$ for $Ti_3C_2Br_2$, $135\,mAhg^{-1}$ for $Ti_3C_2I_2$, $117.2\,mAhg^{-1}$ for Ti_3C_2(BrI), and $106.7\,mAhg^{-1}$ for Ti_3C_2(ClBrI). In addition, $Ti_3C_2Br_2$ and $Ti_3C_2I_2$ showed good cycling stability for 700 and 1000 rounds respectively.

Li et al.[96] constructed a composite with Ti_3C_2 matrices embedded with $M(II)(OH)_n$ (M= Fe, Co, Ni) particles. The $Co(II)(OH)_n@Ti_3C_2$ electrode maintained a specific capacity of $81.1\,mAhg^{-1}$ at $0.1\,Ag^{-1}$ after 600 cycles and had almost 100% coulombic efficiency when used in hybrid Mg-Li batteries. In addition, Zhao et al.[97] synthesized a $Co_3S_4@Ti_3C_2T_x$ cathode for Mg-S batteries. Through both experimental and computational methods, the authors found that the use of the MXene enhances the Mg ion's kinetics, while the electrode had an initial specific capacity of $1220\,mAhg^{-1}$ at 2 C and retained $528\,mAhg^{-1}$ of it after 100 cycles.

Zhao et al.[98] single-atom-doped the Ti_3C_2 MXene with Se and examined it as cathode in Li-O_2 batteries. They found that the material had very high discharge capacity of $17,260\,mAhg^{-1}$ at $0.1\,Ag^{-1}$ and lasting for up to 170 cycles. In addition, Wang et al.[99] used a Ti_3C_2–MnO_2 film for cathode in a Li-CO_2 battery. The electrode had good cycling stability for 220 cycles and had an initial capacity up to $5722\,mAhg^{-1}$ at $0.1\,Ag^{-1}$.

Lu et al.[100], studying Na-Se batteries with computational methods, used a Se@S-P-Ti_3C_2 cathode, i.e., a sulfur-terminated porous Ti_3C_2 MXene. They found that the electrode had a Se capacity of $765\,mAhg^{-1}$ at $0.1\,Ag^{-1}$, 1.2 times higher than the bare porous Ti_3C_2. In addition, it had a very good cycling stability for over 2300 cycles at $0.02\,Ag^{-1}$.

Reddy et al.[101] fabricated a TiO_2-Ti_3C_2 layered structure using a hydrothermal process to use in Na-S batteries. The proposed material had $650\,mAhg^{-1}$ at 1 C initial S capacity, retaining $255.196\,mAhg^{-1}$ after 1500 cycles.

Finally, Han et al.[102] designed a CoS_2@$Ti_3C_2T_x$ cathode via *in situ* hydrothermal growth for use in solid state Zn-air batteries. The authors stated that the electrode showed excellent stability for 60 cycles lasting for 20 hours.

B. 2022

In 2022, Gao et al.[103] studied the conjugated quinone/$Ti_3C_2T_x$ hybrid for cathode electrode in Na-ion batteries. Conjugated quinones, which are a group of organic compounds consisting of a benzene core on which two hydrogen atoms are replaced by two oxygen atoms[104], in general have limited capacity. The addition of the MXene, however, was found both experimentally and through computational methods to build conductive pathways in the material, while the capacity of the electrode was 242 $mAhg^{-1}$ at 0.1 Ag^{-1}.

Moreover, Wu et al.[105] proposed the use of the Ti_3C_2 MXene as a structure for the BDTO anthraquinone derivative in order to synthesize a cathode material for Al-ion batteries. The constructed electrode, Ti_3C_2@BDTO, had an initial capacity of 229.8 $mAhg^{-1}$ at 0.5 Ag^{-1}, maintaining 134.9 $mAhg^{-1}$ of it after 500 cycles, while the BDTO on its own had an initial capacity of 118 $mAhg^{-1}$ at the same current density. The use of the MXene, therefore, improved the electrode's performance.

Geng et al.[106] synthesized a $Ti_3C_2T_x$/carbon nanocage/S cathode for use in Lithium-Sulfur batteries. The materials, which had 80% concentration of sulfur, exhibited a specific capacity of 1275.5 $mAhg^{-1}$ at 0.1 Ag^{-1}, retaining it by 64.6% (823.8 $mAhg^{-1}$) after 100 cycles. This fact indicated that the MXene can adsorb polysulfides so that the battery can have a long-term cyclic stability.

Huang et al.[107] fabricated a polyimede (PI) cathode with PI acting as coating and $Ti_3C_2T_x$ MXene as the matrix and examined it in Li-ion batteries. The PI@$Ti_3C_2T_x$ cathode electrode showed that, when the concentration of the MXene was 5%, it had a capacity of 115 $mAhg^{-1}$ at 0.05 Ag^{-1} which decreased as the current density increased. However, when the MXene concentration was larger (10%), the cathode's capacity exhibited an anomalous behaviour, with it being lower than the 5% case at 0.05 Ag^{-1} - 0.5 Ag^{-1} but larger at 1 Ag^{-1} - 2 Ag^{-1}. The authors attributed this fact to the reduced amount of carbonyl sites at low current rates in the 10% MXene case because of the dense pores in the structure.

Zhai et al.[108] fabricated a FeOF/$Ti_3C_2T_x$ composite for use as cathode in Li-ion batteries. The electrode exhibited an initial specific capacity of 365.5 $mAhg^{-1}$ at 0.1 Ag^{-1} and 202.6 $mAhg^{-1}$ at 2 Ag^{-1} after 400 cycles. In addition, Li et al.[109] synthesized positively charged, pillared Ti_3C_2 as cathode electrode in hybrid Mg-Li batteries. They found that, in All-Phenyl Complex/LiCL (APCL) electrolytes, the electrodes had reversible capacity of 115.9 $mAhg^{-1}$ at 0.1 Ag^{-1}, while in APC electrolytes it had only 60 $mAhg^{-1}$ at 0.1 Ag^{-1}. The rate capability in APCL was 96.3 $mAhg^{-1}$ at 1 Ag^{-1} after 1000 cycles. Furthermore, the presence of the MXene enhanced the Mg ion's kinetics.

Wang et al.[110] designed a single-atom-loaded $Ti_3C_2O_2$ (SA@$Ti_3C_2O_2$) for cathode in aluminum–sulfur batteries. They found that when the single atom is Y, Nb, Mo, or Tc, the reaction energy barrier was as low as 0.23 eV, thus having four cathode electrodes with high performance. In addition, Du et al.[111] designed a g-C_3N_4/$Ti_3C_2T_x$ for Al-ion batteries, where "g" stands for "graphitic". Using density functional theory calculations, the author's showed that the electrode had initial specific capacity of 174 $mAhg^{-1}$ at 4 Ag^{-1}, retaining 75 $mAhg^{-1}$ after 1000 cycles.

Zhu et al.[112] synthesized a cathode electrode based on the C-coated Ti_3C_2 MXene with VS_4 nanosheets generated on it. The VS_4@Ti_3C_2/C electrode had an initial Mg specific capacity of 498 $mAhg^{-1}$ at 0.5 Ag^{-1}, falling to 147 $mAhg^{-1}$ at 0.5 Ag^{-1} after 900 cycles, a value still high when the VS_4 on reduced graphene oxide delivers only an initial 123.8 $mAhg^{-1}$ at 0.5 Ag^{-1} and fades fast after only 200 cycles. In addition, Feng et al.[113] designed a Zn-ion battery with a VS_2/$Ti_3C_2T_x$ cathode and a Zn/$Ti_3C_2T_x$ anode. They found that the cathode electrode had an initial capacity of 213.4 $mAhg^{-1}$ at 0.2 Ag^{-1}, maintaining 93.4% of it after 2400 cycles. In addition, Feng et al. checked the flexibility of the battery by bending it to various degrees. They showed that, when the battery is bent to 90°, i.e., bent to the maximum, it retained 99.5% of its initial performance, a fact that can be attributed to the presence of the MXene.

Lv et al.[114] synthesized the V_2C MXene and calcinated it with Se. The V_2C@Se electrode was tested in aluminum-ion batteries and it was found to have an initial specific capacity of 402.5 $mAhg^{-1}$ at 1 Ag^{-1}, retaining 119.8 $mAhg^{-1}$ of it after 1000 cycles. Moreover, Xu et al.[115] fabricated the V_2C MXene with oxygen terminated atoms for use in Li-O_2 batteries. The V_2CO_2 cathode had a superior capacity of 8577.3 $mAhg^{-1}$ at 0.1 Ag^{-1}, maintaining cycling stability for 302 cycles.

Du et al.[116] designed a 3D VN/$Ti_3C_2T_x$ composite for use in Zn-ion batteries, by encapsulating microspheres of VN into the MXene. The cathode had an initial capacity of 521 $mAhg^{-1}$ at 0.5 Ag^{-1} when the pure VN had only 324 $mAhg^{-1}$ after 100 cycles. In addition, the VN/$Ti_3C_2T_x$ electrode maintained 371.2 $mAhg^{-1}$ at 0.5 Ag^{-1} after 140 cycles, whereas in the high current density of 5 Ag^{-1} the cycling stability lasted for 2000 cycles.

Zhao et al.[117] synthesized an M-$Ti_3C_2T_x$@MoS_2@C electrode, i.e., a monolayer (M) $Ti_3C_2T_x$ MXene with MoS_2 nanosheets embedded on its surface and a carbon layer coated on top of all. The electrode, when used as a cathode in Li-ion batteries, had an initial capacity of 724.9 $mAhg^{-1}$ at 2 Ag^{-1}, and, after 1000 cycles, 764 $mAhg^{-1}$ at 0.5 Ag^{-1}.

Shi et al.[118] synthesized a MoO_3/$Ti_3C_2T_x$ cathode for

use in Zn-ion batteries. The presence of the MXene reduces the hydrophilicity of the molybdenum trioxide and helped to stop the dissolution of the cathode. The electrode had an initial specific capacity of 369.8 $mAhg^{-1}$ at 0.2 Ag^{-1}, retaining it by 46.7% after 1600 cycles.

Dong et al.[119] designed an MXene-Carbon Nanotube-Cellulose-$LiFePO_4$ cathode for Li-ion batteries (MCC-LFP) with the $Ti_3C_2T_x$ MXene as the key material. The electrode showed specific capacity attenuation at high current densities, but it achieved 152 $mAhg^{-1}$ at 0.5 C (1 C=170 mAg^{-1}) when the mixture had the composition of 20 mg $Ti_3C_2T_x$, 10 mg carbon nanotubes and $10 - 20$ mg cellulose.

Also in 2022, Zhao et al.[120] proposed an S@MCS-SiO2/$Ti_3C_2T_x$ cathode, where MCS stands for Mesoporous Carbon Nanospheres, for Li-S batteries. The MXene managed to confine the highly soluble polysulfides, enhancing the electrode's stability. In addition, the cathode exhibited an initial specific capacity of 1303.6 $mAhg^{-1}$ at 0.1 C, with a decay rate of 0.046% per cycle in the first 1000 cycles.

Liang et al.[121] synthesized a $H_2V_3O_8/Ti_3C_2T_x$ composite for cathode electrode in Zn-ion batteries. The material had an initial specific capacity of 420 $mAhg^{-1}$ at 10 Ag^{-1}, while the authors report an outstanding performance with a 323 $mAhg^{-1}$ capacity at 10 Ag^{-1} for over 9000 cycles. In addition, density functional theory calculations showed that the energy barrier for diffusion of a Zn ion in the $H_2V_3O_8/Ti_3C_2T_x$ composite was 1.3 eV. This value, although high, it is still lower than the 3.4 eV in $H_2V_3O_8$, indicating that the addition of the MXene improved the Zn ion's kinetics.

Yang et al.[122] studied theoretically the Ti_3C_2 MXene with F, O, OH terminations for the cathode electrode in Li-O_2 batteries. They found that the oxygen termination atoms significantly enhance the material's catalytic behaviour.

Li et al.[123] grew $VO(CH_2O)_2$ (vanadyl ethylene glycolate) on the $Ti_3C_2T_x$ MXene using an oil-bath heating process. The $VO(CH_2O)_2@Ti_3C_2T_x$ electrode, when used in Zn-ion batteries, exhibited an initial capacity of 360.3 $mAhg^{-1}$ capacity at 0.5 Ag^{-1} retaining it by 90.7% for 200 cycles. In addition, in the higher current density of 10 Ag^{-1}, the cathode had 85.2% capacity retention after 3000 cycles (137.6 $mAhg^{-1}$).

Huo et al.[124] used a few layers of the $Ti_3C_2T_x$ MXene and loaded Te on its surface, using an evaporation in high temperatures method, in order to examine its performance as a cathode in an Al ion battery. The $Ti_3C_2T_x$@Te electrode had an initial specific capacity of 987 $mAhg^{-1}$ at 0.2 Ag^{-1} with Te as the active material. Furthermore, after 150 cycles at 0.6 Ag^{-1} current density, the specific capacity fell to 449 $mAhg^{-1}$.

Pai et al.[125] confined S_8 in the $Ti_3C_2T_x$ MXene by increasing the MXene's interlayer spacing with the use of di (hydrogenated tallow) benzyl methyl ammonium chloride (DHT). The- $Ti_3C_2T_x/S_8$ composite was then tested as cathode in alkali metal-sulfur batteries. Te electrode exhibited an initial capacity of 1100 $mAhg^{-1}$ at 0.1 C for Li-S batteries, retaining 550 $mAhg^{-1}$ at 0.5 C after 1000 cycles. In addition, when using a Na anode, i.e., for a Na-S battery, the electrode had initial capacity 1400 $mAhg^{-1}$ at 0.05 C, retaining 600 $mAhg^{-1}$ at 0.5 C after 400 cycles. Finally, in a K-S battery, the cathode exhibited an initial capacity of 1700 $mAhg^{-1}$ at 0.05 C, delivering 400 $mAhg^{-1}$ at 0.1 C after 400 cycles. Here, 1 C was equal to 1675 mAg^{-1}. Therefore, the Li-S system seems to have the best cycling stability, however, the $Ti_3C_2T_x/S_8$ electrode could present as a universal solution for alkali metal-sulfur batteries, as Pai et al. suggest.

In Table III we summarize the specific capacities and performance rates for the cathode electrodes. It is evident that Ti-based MXenes are predominantly used, while the Nb_2CO_2 exhibits the highest initial capacity, i.e., $19,785.5$ $mAhg^{-1}$ at 0.2 Ag^{-1}.

IV. CONCLUDING REMARKS & FUTURE WORK

In Figure 3 we can see an analysis of the anode materials and the battery types discussed in Section II.

The $Ti_3C_2T_x$ is the most commonly used MXene for anode electrode, with 67% of anode materials being Ti-based. This stands to reason, considering that $Ti_3C_2T_x$ is the most conductive MXene out of all experimentally discovered[6–8]. In addition, whether the mobile ion has a low energy barrier for diffusion is the most examined criterion for considering an MXene as a suitable material for negative electrode in secondary batteries. It is expected, therefore, to use materials that have already exhibited high ionic and electronic conductivity.

One of the most important problems when it comes to experimentally synthesizing MXenes is the fact that there are not enough precursory MAX phases[126] to etch them from. This problem was addressed when, in 2016, Zhou et al.[127] managed to synthesize the zirconium carbide MXene from a layered ternary transition metal carbide ($Zr_3Al_3C_5$), i.e., without the use of a MAX phase[50]. Still, however, the use of Zr-based materials for anodes amounts only to 4% of the cases described in this study, and those cases are mostly theoretical. It would be advantageous, therefore, to have a more widespread practical application of the Zr-based materials for anode electrodes.

Regarding the battery types used in the search of promising anode materials, Li-ion batteries are the most predominantly used (46%, see Fig. 3), despite the fact that there are major disadvantages when it comes to them. First of all, there is a limitation in recent years in Li natural reserves[128]. In addition, Li-ion batteries have not been applicable to large-scale applications yet[8,129], but only to portable devices like laptops and cell phones[130]. Finally, the lithium-dendrite formation[131] is a safety issue that has yet to be bypassed, making the batteries flammable and shortening their lifetime. Per-

TABLE III: Specific capacities and rate capabilities in literature for the years 2021-2022 (alphabetically by material) for cathode electrodes.

Cathode	Battery Type	Current Rate	Initial Capacity ($mAhg^{-1}$)	Rate Capability	Durability (Cycles)	Reference
Co-$MoSe_2$/$Ti_3C_2T_x$	Li-S	0.1 C	1454	-	-	[82]
Co(II)$(OH)_n$@Ti_3C_2	Mg-Li	-	-	81.1 $mAhg^{-1}$ at 0.1 Ag^{-1}	600	[96]
Co_3S_4@$Ti_3C_2T_x$	Mg-S	2 C	1220	528 $mAhg^{-1}$ at 2 C	100	[97]
CoS_2@$Ti_3C_2T_x$	Zn-air	-	-	-	60	[102]
FeOF/$Ti_3C_2T_x$	Li-ion	0.1 Ag^{-1}	365.5	202.6 $mAhg^{-1}$ at 2 Ag^{-1}	400	[108]
g-C_3N_4/$Ti_3C_2T_x$	Al-ion	4 Ag^{-1}	174	75 $mAhg^{-1}$ at 4 Ag^{-1}	1000	[111]
graphene/$Ti_3C_2T_x$@S	Li-S	0.1 C	1483.1	at 1 C	1000	[86]
$H_2V_3O_8$/$Ti_3C_2T_x$	Zn-ion	10 Ag^{-1}	420	323 $mAhg^{-1}$ at 10 Ag^{-1}	9000	[121]
$H_2V_3O_8$/$Ti_3C_2T_x$	Zn-ion	0.2 Ag^{-1}	305.3	at 5 Ag^{-1}	5600	[91]
$LiFePO_4$@$Ti_3C_2T_x$	Li-ion	-	-	94.8%	500	[77]
M-$Ti_3C_2T_x$@MoS_2@C	Li-ion	2 Ag^{-1}	724.9	764 $mAhg^{-1}$ at 0.5 Ag^{-1}	1000	[117]
MCC-LFP	Li-ion	0.5 C	152	-	-	[119]
MoO_3/$Ti_3C_2T_x$	Zn-ion	0.2 Ag^{-1}	309.8	46.7%	1600	[118]
MoS_2/$Ti_3C_2T_x$	Al-ion	-	-	166 $mAhg^{-1}$	60	[89]
Nb_2CO_2	Li-O	0.2 Ag^{-1}	19785.5	at 3 Ag^{-1}	130	[80]
PDDA/$Ti_3C_2T_x$	Li-S	0.2 C	1016.8	-	-	[84]
PI@$Ti_3C_2T_x$	Li-ion	0.05 Ag^{-1}	115	-	-	[107]
quinone/$Ti_3C_2T_x$	Na-ion	0.1 Ag^{-1}	242	-	-	[103]
S@MCS-SiO2/$Ti_3C_2T_x$	Li-S	0.1 C	1303.6	-	1000	[120]
S/$Ti_3C_2T_x$-CS_2/IPA	Li-S	0.1 Ag^{-1}	1474.5	522.7 $mAhg^{-1}$ at 1 Ag^{-1}	1000	[87]
S/$Ti_3C_2T_x$	Li-S	0.5 C	1277	1059 $mAhg^{-1}$ at 0.5 C	100	[88]
Se/Ti_3C_2	Li-O_2	0.1 Ag^{-1}	17260	-	170	[98]
Se@S-P-Ti_3C_2	Na-Se	0.1 Ag^{-1}	765	at 0.02 Ag^{-1}	2300	[100]
Ti_3C_2-MnO_2	Li-CO_2	0.1 Ag^{-1}	5722	-	220	[99]
Ti_3C_2@BDTO	Al-ion	0.5 Ag^{-1}	229.8	134.9 $mAhg^{-1}$ at 0.5 Ag^{-1}	500	[105]
Ti_3C_2	Mg-Li	0.1 Ag^{-1}	115.9	96.3% at 1 Ag^{-1}	1000	[109]
Ti_3C_2(BrI)	Zn-ion	0.5 Ag^{-1}	117.2	-	-	[95]
Ti_3C_2(ClBrI)	Zn-ion	0.5 Ag^{-1}	106.7	-	-	[95]
$Ti_3C_2Br_2$	Zn-ion	0.5 Ag^{-1}	97.9	-	700	[95]
$Ti_3C_2Cl_2$	Zn-ion	0.5 Ag^{-1}	46.5	-	-	[95]
$Ti_3C_2I_2$	Zn-ion	0.5 Ag^{-1}	135	-	1000	[95]
$Ti_3C_2T_x$@Te	Al-ion	0.2 Ag^{-1}	987	449 $mAhg^{-1}$ at 0.6 Ag^{-1}	150	[124]
$Ti_3C_2T_x$/S_8	K-S	0.05 C	1700	400 $mAhg^{-1}$ at 1 C	400	[125]
$Ti_3C_2T_x$/S_8	Li-S	0.1 C	1100	550 $mAhg^{-1}$ at 0.5 C	1000	[125]
$Ti_3C_2T_x$/S_8	Na-S	0.05 C	1400	600 $mAhg^{-1}$ at 0.5 C	400	[125]
$Ti_3C_2T_x$	Li-S	-	-	-	300	[81]
$Ti_3C_2T_x$/carbon nanocage/S	Li-S	0.1 Ag^{-1}	1275.5	64.6%	100	[106]
TiO_2-Ti_3C_2	Na-S	1 C	650	255.196 $mAhg^{-1}$ at 1 C	1500	[101]
V_2C	Zn-ion	-	423.5	-	-	[92]
V_2C@Se	Al-ion	1 Ag^{-1}	402.5	119.8 $mAhg^{-1}$ at 1 Ag^{-1}	1000	[114]
V_2C-O	Li-O_2	0.1 Ag^{-1}	8577.3	-	302	[115]
V_2CT_x	Zn-ion	0.05 Ag^{-1}	118.5	-	-	[93]
V_2O_5/$Ti_3C_2T_x$	Li-ion	1 C	321	91.8% at 10.5 C	680	[41]
VN/$Ti_3C_2T_x$	Zn-ion	0.5 Ag^{-1}	521	371.2 $mAhg^{-1}$ at 0.5 Ag^{-1}	140	[116]
VN/$Ti_3C_2T_x$	Zn-ion	0.5 Ag^{-1}	521	at 5 Ag^{-1}	2000	[116]
$VO(CH_2O)_2$@$Ti_3C_2T_x$	Zn-ion	0.5 Ag^{-1}	360.3	90.7%	200	[123]
$VO(CH_2O)_2$@$Ti_3C_2T_x$	Zn-ion	0.5 Ag^{-1}	360.3	85.2% at 10 Ag^{-1}	3000	[123]
VO_2/$Ti_3C_2T_x$	Zn-ion	0.2 Ag^{-1}	228.5	72.1%	2500	[90]
VS_2/$Ti_3C_2T_x$	Zn-ion	0.2 Ag^{-1}	213.4	93.4%	2400	[113]
VS_4@Ti_3C_2/C	Mg-ion	0.5 Ag^{-1}	498	147 $mAhg^{-1}$ at 0.5 Ag^{-1}	900	[112]

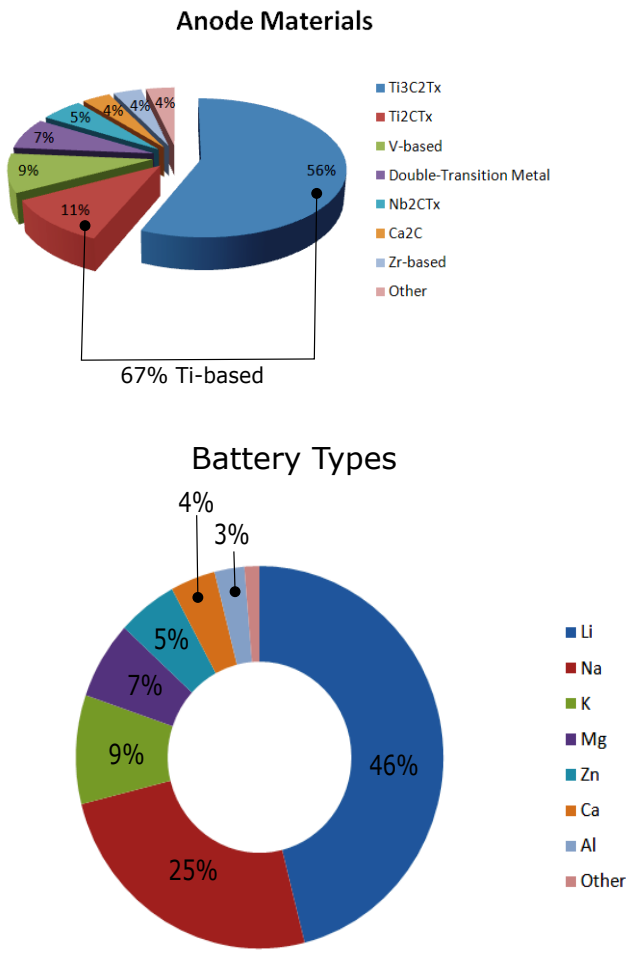

FIG. 3: Most commonly used anode materials and battery types.

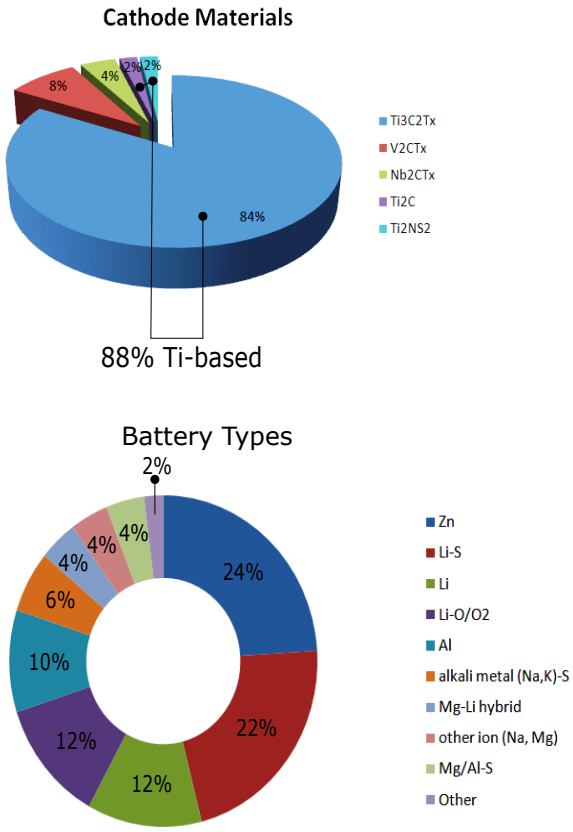

FIG. 4: Most commonly used cathode materials and battery types.

haps for these reasons, there is a concentrated effort to turn the attention to other types of ion batteries during the last two years.

After lithium-ion batteries, the Na-ion ones have seen a rising in cases (25%, see Fig. 3), while another 46% from the total number of cases have used an ion battery different than the Li one (25% Na-ion, 9% K-ion, 7% Mg-ion, 5% Zn-ion, see Fig. 3). Considering that multivalent atom-batteries like Mg have the extra advantage of providing higher energy density[132] and volumetric capacity[131], however, it could be useful to have this type of batteries more thoroughly examined.

Regarding the cathode materials, the trend of Ti-based MXenes remains strong, with a staggering 84% of all cases discussed in this review using the $Ti_3C_2T_x$ MXene as positive electrode (see Fig. 4).

However, while the main criterion for enhancing battery performance was the mobility of the ion when it came to the anodes, for the cathodes the community is more concerned with the specific capacity of the materials used, as well as their durability (the amount of charging/discharging cycles they can undergo before the capacity falls to a certain percentage of the nominal capacity). Perhaps it is for this reason that we observe a turn away from Li-ion batteries (12%, see Fig. 4), and focus on Zn-ion ones (24%, see Fig. 4). The Zn ion is divalent (Zn^{2+}), therefore there are two electrons involved in the intercalation of each ion in the cathode material, and that doubles the capacity per unit volume when compared to ions like Li^+, Na^+ and K^+. Furthermore, the Al-ion batteries (Al^{3+}) have also seen a rise, with 10% of the studies regarding cathode materials using them (see Fig. 4).

A close second (22% of all cathode cases, see Fig. 4) is the lithium-sulfur batteries (Li anode and S cathode). Li-S batteries have higher energy density than the Li-ion ones[133]. In addition, S is in abundance in the earth's crust[133], therefore Li-S batteries have lower cost for production. Despite these advantages however, Li-S batteries are far from being commercially viable because of the existence of the polysulfides and the shuttle effect[134], i.e., the diffusion of lithium polysulfides and their dissolution in the electrolyte, which leads to loss of S and rapid capacity decay[135]. Furthermore, S exhibits low conductivity and slow kinetics[136], which can be improved with the use of MXenes.

Finally, Li-air ($Li\text{-}O/LiO_2$) have also substantially been used (12%, see Fig. 4), due to their increased

specific energy, and the use of safe, non-flammable electrolytes[137].

Numerous reports are published yearly regarding the use of MXenes as anode and cathode electrodes in secondary batteries. Here, we report on the last two years' (2021-2022) studies, but despite the very promising results, there is still another issue that needs to be overcome: MXenes without termination atoms, i.e., bare MXenes have yet to be synthesized. Considering that the termination atoms affect the electronic properties of the MXenes[8,138,139], it would be prudent to explore more methods to manipulate the termination atoms.

Finally, the durability of MXenes is a problem that needs addressing, since MXenes degrade fast in water and air, thus limitng their use[140].

Data Availability

Data sharing is not applicable to this article as no new data were created or analyzed in this study.

Conflict of Interest

The authors have no conflicts to disclose.

* Electronic address: S.R.Christopoulos@hud.ac.uk

[1] M. Naguib, M. Kurtoglu, V. Presser, J. Lu, J. Niu, M. Heon, L. Hultman, Y. Gogotsi, and M. W. Barsoum, Advanced Materials **23**, 4248 (2011).

[2] M. W. Barsoum and T. El-Raghy, American Scientist **89**, 334 (2001).

[3] Z. Sun, International Materials Reviews **56**, 143 (2011).

[4] M. Radovic and M. W. Barsoum, American Ceramics Society Bulletin **92**, 20 (2013).

[5] A. Jain, S. P. Ong, G. Hautier, W. Chen, W. D. Richards, S. Dacek, S. Cholia, D. Gunter, D. Skinner, and G. Ceder, APL Materials **1**, 011002 (2013).

[6] J. Zhu, A. Chroneos, and U. Schwingenschlögl, Physica Status Solidi (RRL)–Rapid Research Letters **9**, 726 (2015).

[7] C. J. Zhang, S. Pinilla, N. McEvoy, C. P. Cullen, B. Anasori, E. Long, S.-H. Park, A. Seral-Ascaso, A. Shmeliov, D. Krishnan, et al., Chemistry of Materials **29**, 4848 (2017).

[8] K. A. Papadopoulou, A. Chroneos, D. Parfitt, and S.-R. G. Christopoulos, Journal of Applied Physics **128**, 170902 (2020).

[9] J. L. Hart, K. Hantanasirisakul, A. C. Lang, B. Anasori, D. Pinto, Y. Pivak, J. T. van Omme, S. J. May, Y. Gogotsi, and M. L. Taheri, Nature Communications **10**, 1 (2019).

[10] C. Liao, in *Batteries* (IOP Publishing, 2021), 2053-2563, pp. 1–1 to 1–24, ISBN 978-0-7503-2682-7, URL `https://dx.doi.org/10.1088/978-0-7503-2682-7ch1`.

[11] D. Deng, Energy Science & Engineering **3**, 385 (2015).

[12] H. A. Kiehne, *Battery technology handbook*, vol. 118 (CRC Press, 2003).

[13] B. Kang and G. Ceder, Nature **458**, 190 (2009).

[14] M. Team et al., Massachusetts Institute of technology, USA, Tech. Rep. (2008).

[15] S. Megahed and B. Scrosati, Journal of Power Sources **51**, 79 (1994).

[16] D. Deng and J. Y. Lee, ACS Applied Materials & Interfaces **6**, 1173 (2014).

[17] N. Dimov, Y. Xia, and M. Yoshio, Journal of Power Sources **171**, 886 (2007).

[18] M. Winter and J. O. Besenhard, Electrochimica Acta **45**, 31 (1999).

[19] P. Poizot, S. Laruelle, S. Grugeon, L. Dupont, and J. Tarascon, Nature **407**, 496 (2000).

[20] K. Charette, J. Zhu, S. O. Salley, K. S. Ng, and D. Deng, RSC Advances **4**, 2557 (2014).

[21] X. Wang and L. Bannenberg, MRS Bulletin **46**, 755 (2021).

[22] Y. Li, L. Li, R. Huang, Y. Zhang, and Y. Wen, Nanoscale **13**, 2995 (2021).

[23] Z. Xia, X. Chen, H. Ci, Z. Fan, Y. Yi, W. Yin, N. Wei, J. Cai, Y. Zhang, and J. Sun, Journal of Energy Chemistry **53**, 155 (2021).

[24] S. Zhong, S. Ju, Y. Shao, W. Chen, T. Zhang, Y. Huang, H. Zhang, G. Xia, and X. Yu, Journal of Energy Chemistry **62**, 431 (2021).

[25] A. Saha, N. Shpigel, N. Leifer, S. Taragin, T. Sharabani, H. Aviv, I. Perelshtein, G. D. Nessim, M. Noked, and Y. Gogotsi, Advanced Functional Materials **31**, 2106294 (2021).

[26] K. A. Papadopoulou, D. Parfitt, A. Chroneos, and S.-R. G. Christopoulos, Journal of Applied Physics **130**, 095101 (2021).

[27] R. Cheng, T. Hu, Z. Wang, J. Yang, R. Dai, W. Wang, C. Cui, Y. Liang, C. Zhang, C. Li, et al., Physical Chemistry Chemical Physics **23**, 23173 (2021).

[28] K. Rajput, V. Kumar, S. Thomas, M. A. Zaeem, and D. R. Roy, 2D Materials **8**, 035015 (2021).

[29] P. A. Maughan, L. Bouscarrat, V. R. Seymour, S. Shao, S. J. Haigh, R. Dawson, N. Tapia-Ruiz, and N. Bimbo, Nanoscale Advances **3**, 3145 (2021).

[30] N. Zhao, Y. Yang, D. Yi, Y. Xiao, K. Wang, W. Cui, and X. Wang, Chemical Engineering Journal **422**, 130018 (2021).

[31] H. Ma, J. Li, J. Yang, N. Wang, Z. Liu, T. Wang, D. Su, C. Wang, and G. Wang, Chemistry–An Asian Journal **16**, 3774 (2021).

[32] F. Wang, X. Ma, P. Zou, G. Wang, Y. Xiong, Y. Liu, F. Ren, and X. Xiong, Surface and Coatings Technology **422**, 127568 (2021).

[33] L. Gou, W. Jing, Y. Li, M. Wang, S. Hu, H. Wang, and Y.-B. He, ACS Applied Energy Materials **4**, 7268 (2021).

[34] K. Liang, A. Tabassum, A. Majed, C. Dun, F. Yang, J. Guo, K. Prenger, J. J. Urban, and M. Naguib, InfoMat **3**, 1422 (2021).

[35] X. Wang, Y. Wang, Y. Jiang, X. Li, Y. Liu, H. Xiao, Y. Ma, Y.-y. Huang, and G. Yuan, Advanced Functional

Materials **31**, 2103210 (2021).
[36] Y. Dong, Z. Tang, P. Liang, H. Wan, H. Wang, L. Wang, H. Shu, and D. Chao, Journal of Colloid and Interface Science **593**, 51 (2021).
[37] P. P. Dinda and S. Meena, Journal of Physics: Condensed Matter **33**, 175001 (2021).
[38] Y. Chen, Y. Sun, M. Geng, W. Shao, Y. Chen, X. Liu, and M. Ou, Materials Letters **304**, 130704 (2021).
[39] M. Zhu, X. Deng, Z. Feng, M. He, Y. Feng, and D. Xiong, Journal of Alloys and Compounds **886**, 161139 (2021).
[40] H. Dong, P. Xiao, N. Jin, B. Wang, Y. Liu, and Z. Lin, ChemElectroChem **8**, 957 (2021).
[41] S. Wang, Y. Liu, K. Lu, W. Cai, Y. Jie, F. Huang, X. Li, R. Cao, and S. Jiao, Energy & Fuels **35**, 4587 (2021).
[42] Y. Chen, Z. Pu, Y. Liu, Y. Shen, S. Liu, D. Liu, and Y. Li, Journal of Power Sources **515**, 230601 (2021).
[43] Y. Tian, Y. An, C. Liu, S. Xiong, J. Feng, and Y. Qian, Energy Storage Materials **41**, 343 (2021).
[44] W. Fan, J. Xue, D. Wang, Y. Chen, H. Liu, and X. Xia, ACS Applied Materials & Interfaces **13**, 61055 (2021).
[45] Y. Guo, D. Zhang, Y. Yang, Y. Wang, Z. Bai, P. K. Chu, and Y. Luo, Nanoscale **13**, 4624 (2021).
[46] X.-H. Zha, X. Ma, J.-T. Luo, and C. Fu (2022).
[47] Y. Zhu, S. Zheng, P. Lu, J. Ma, P. Das, F. Su, H.-M. Cheng, and Z.-S. Wu, National Science Review **9** (2022).
[48] U. Alli, K. McCarthy, I.-A. Baragau, N. P. Power, D. J. Morgan, S. Dunn, S. Killian, T. Kennedy, and S. Kellici, Chemical Engineering Journal **430**, 132976 (2022).
[49] K. A. Papadopoulou, A. Chroneos, and S.-R. G. Christopoulos, Journal of Physics and Chemistry of Solids p. 110713 (2022).
[50] K. A. Papadopoulou, A. Chroneos, and S.-R. G. Christopoulos, Journal of Alloys and Compounds p. 166240 (2022).
[51] Y. Shi, D. Zhou, T. Wu, and Z. Xiao, ACS Applied Materials & Interfaces **14**, 29905 (2022).
[52] H. Liu, Y. Cai, Z. Guo, and J. Zhou, ACS Omega **7**, 17756 (2022).
[53] Z. Guo, D. Wang, Z. Wang, Y. Gao, and J. Liu, Nanomaterials **12**, 1422 (2022).
[54] H. A. Tariq, U. Nisar, J. J. Abraham, Z. Ahmad, S. AlQaradawi, R. Kahraman, and R. Shakoor, Applied Surface Science **583**, 152441 (2022).
[55] X. Han, W. Zhou, M. Chen, J. Chen, G. Wang, B. Liu, L. Luo, S. Chen, Q. Zhang, S. Shi, et al., Journal of Energy Chemistry **67**, 727 (2022).
[56] Z. Wu, S. Zhu, X. Bai, M. Liang, X. Zhang, N. Zhao, and C. He, Electrochimica Acta **407**, 139916 (2022).
[57] Q. Ma, Z. Zhang, P. Kou, D. Wang, Z. Wang, H. Sun, R. Zheng, and Y. Liu, Journal of Colloid and Interface Science **617**, 147 (2022).
[58] Y. Wu, D. Liu, D. Qu, J. Li, Z. Xie, X. Zhang, H. Chen, and H. Tang, Chemical Engineering Journal **438**, 135328 (2022).
[59] Y. Wang, Y. Ma, Q. Zhang, R. Huang, B. Gao, Z. Li, G. Li, and F. Liang, Current Applied Physics **41**, 7 (2022).
[60] X. Zhang, T. Zhang, C. Zhang, J. Xiao, D. Wu, X. Ma, and H. Gao, Journal of Alloys and Compounds **909**, 164730 (2022).
[61] P. Gong, X. Zhang, F. Liu, K. Yao, and S. Zhu, Surfaces and Interfaces p. 102091 (2022).
[62] Y. Qian, K. Zhang, L. Tan, Y. An, B. Xi, S. Xiong, J. Feng, and Y. Qian, Chemical Engineering Journal **440**, 135818 (2022).
[63] C. Wei, T. Fang, X. Tang, K. Jiang, and X. Liu, Langmuir (2022).
[64] J. Zhou, M. Xie, F. Wu, Y. Mei, Y. Hao, L. Li, and R. Chen, Advanced Materials **34**, 2106897 (2022).
[65] K. Yuan, P. Hao, X. Hu, J. Zhang, and Y. Zhou, Journal of Materials Science **57**, 7001 (2022).
[66] H. Zhang, J. Song, J. Li, J. Feng, Y. Ma, L. Ma, H. Liu, Y. Qin, X. Zhao, and F. Wang, ACS Applied Materials & Interfaces **14**, 16300 (2022).
[67] D. Seo, M.-R. Kim, J. Kyu Song, E. Kim, J. Koo, K.-C. Kim, H. Han, Y. Lee, and C. Won Ahn, ChemElectroChem **9**, e202101344 (2022).
[68] Q. Deng, M. Wang, X. Liu, H. Fan, Y. Zhang, and H. Y. Yang, Journal of Colloid and Interface Science **626**, 700 (2022).
[69] X. He, Y. Ni, Y. Li, H. Sun, Y. Lu, H. Li, Z. Yan, K. Zhang, and J. Chen, Advanced Materials **34**, 2106565 (2022).
[70] M. L. Carvalho, G. Mela, A. Temporelli, E. Brivio, and P. Girardi, Sustainability **14**, 5976 (2022).
[71] T. Ghaed-Sharaf and A. Omidvar, Physical Chemistry Chemical Physics (2022).
[72] C. Liu, J. Zhou, X. Li, Z. Fang, R. Sun, G. Yang, and W. Hou, Chemical Engineering Journal **431**, 133838 (2022).
[73] Y. Qian, Y. An, Y. Zhang, C. Wei, B. Xi, S. Xiong, and J. Feng, Journal of Power Sources **520**, 230901 (2022).
[74] C. Cui, R. Dai, C. Zhang, B. Fan, and X. Wang, Journal of Materials Chemistry A **10**, 15474 (2022).
[75] C. Zhao, Z. Wei, J. Zhang, P. He, X. Huang, X. Duan, D. Jia, and Y. Zhou, Journal of Alloys and Compounds **907**, 164428 (2022).
[76] K. Tian, X. Hui, H. Wang, Z. Zhang, L. Zhang, C. Wang, and L. Yin, Electrochimica Acta **415**, 140242 (2022).
[77] H. Zhang, J. Li, L. Luo, J. Zhao, J. He, X. Zhao, H. Liu, Y. Qin, F. Wang, and J. Song, Journal of Alloys and Compounds **876**, 160210 (2021).
[78] X. Li, X. Ma, Y. Hou, Z. Zhang, Y. Lu, Z. Huang, G. Liang, M. Li, Q. Yang, J. Ma, et al., Joule **5**, 2993 (2021).
[79] J. Li, K. Han, J. Huang, G. Li, S. Peng, N. Li, J. Wang, W. Zhang, Y. Du, Y. Fan, et al., Energy Storage Materials **35**, 669 (2021).
[80] G. Li, N. Li, S. Peng, B. He, J. Wang, Y. Du, W. Zhang, K. Han, and F. Dang, Advanced Energy Materials **11**, 2002721 (2021).
[81] W. Zhao, Y. Lei, Y. Zhu, Q. Wang, F. Zhang, X. Dong, and H. N. Alshareef, Nano Energy **86**, 106120 (2021).
[82] W. Wang, L. Huai, S. Wu, J. Shan, J. Zhu, Z. Liu, L. Yue, and Y. Li, ACS nano **15**, 11619 (2021).
[83] C. Wei, M. Tian, Z. Fan, L. Yu, Y. Song, X. Yang, Z. Shi, M. Wang, R. Yang, and J. Sun, Energy Storage Materials **41**, 141 (2021).
[84] L. Zhang, J. Bi, Z. Zhao, Y. Wang, D. Mu, and B. Wu, Electrochimica Acta **370**, 137759 (2021).
[85] C. Yao, W. Li, K. Duan, C. Zhu, J. Li, Q. Ren, and G. Bai, Nanomaterials **11**, 2478 (2021).
[86] H. Li, F. Shao, X. Wen, Y. Ding, C. Zhou, Y. Zhang, H. Wei, and N. Hu, Electrochimica Acta **371**, 137838 (2021).
[87] C. Xue, C. Yue, and L. Yuan, Journal of Alloys and Compounds **886**, 161152 (2021).
[88] A. Wang, Y. Chen, L. Liu, X. Liu, Z. Wang, and Y. Zhang, Dalton Transactions **50**, 5574 (2021).

[89] B. Tan, T. Lu, W. Luo, Z. Chao, R. Dong, and J. Fan, Energy & Fuels **35**, 12666 (2021).
[90] Z. Shi, Q. Ru, Z. Pan, M. Zheng, F. Chi-Chun Ling, and L. Wei, ChemElectroChem **8**, 1091 (2021).
[91] C. Liu, W. Xu, C. Mei, M.-C. Li, X. Xu, and Q. Wu, Chemical Engineering Journal **405**, 126737 (2021).
[92] Y. Liu, Y. Jiang, Z. Hu, J. Peng, W. Lai, D. Wu, S. Zuo, J. Zhang, B. Chen, Z. Dai, et al., Advanced Functional Materials **31**, 2008033 (2021).
[93] Y. Li, H. Yang, T. Zhang, S. Li, S. Li, S. He, T. Chen, J. Y. Lee, Y. Zhao, and P.-Y. Chen, Advanced Energy Materials **11**, 2101862 (2021).
[94] Y. Wang, T. Lubbers, R. Xia, Y.-Z. Zhang, M. Mehrali, M. Huijben, and E. Johan, Journal of The Electrochemical Society **168**, 020507 (2021).
[95] M. Li, X. Li, G. Qin, K. Luo, J. Lu, Y. Li, G. Liang, Z. Huang, J. Zhou, L. Hultman, et al., ACS Nano **15**, 1077 (2021).
[96] X. Li, Y. Tang, L. Liu, Y. Gao, C. Zhu, Y. NuLi, and T. Yang, Journal of Materials Science **56**, 2464 (2021).
[97] Q. Zhao, R. Wang, Y. Zhang, G. Huang, B. Jiang, C. Xu, and F. Pan, Journal of Magnesium and Alloys **9**, 78 (2021).
[98] D. Zhao, P. Wang, H. Di, P. Zhang, X. Hui, and L. Yin, Advanced Functional Materials **31**, 2010544 (2021).
[99] Y. Wang, X. Wang, B. Ge, J. Guo, C. Fernandez, and Q. Peng, ACS Applied Energy Materials **4**, 9961 (2021).
[100] C. Lu, A. Li, G. Li, Y. Yan, M. Zhang, Q. Yang, W. Zhou, and L. Guo, Advanced Materials **33**, 2008414 (2021).
[101] B. Reddy, G.-B. Cho, N. Reddy, H.-J. Ahn, J.-H. Ahn, T. Maiyalagan, and K.-K. Cho, Journal of Alloys and Compounds **883**, 160910 (2021).
[102] S. Han, Y. Chen, Y. Hao, Y. Xie, D. Xie, Y. Chen, Y. Xiong, Z. He, F. Hu, L. Li, et al., Science China Materials **64**, 1127 (2021).
[103] Y. Gao, P. Xue, L. Ji, X. Pan, L. Chen, W. Guo, M. Tang, C. Wang, and Z. Wang, ACS Applied Materials & Interfaces **14**, 8036 (2022).
[104] in *Recent Advances in Natural Products Analysis*, edited by A. Sanches Silva, S. F. Nabavi, M. Saeedi, and S. M. Nabavi (Elsevier, 2020), pp. 749–766, ISBN 978-0-12-816455-6.
[105] G. Wu, C. Lv, W. Lv, X. Li, W. Zhang, and Z. Li, Journal of Energy Chemistry **74**, 174 (2022).
[106] X. Geng, C. Liu, Y. Sun, Y. Zhao, R. Yi, P. Song, C. Zhao, I. Mitrovic, L. Yang, and C. Zhao, Journal of Alloys and Compounds **895**, 162586 (2022).
[107] X.-W. Huang, S.-Y. Liao, Y.-Z. Li, C.-S. Liu, W.-X. Cheng, C. Zhao, Y.-Z. Chen, Y.-D. Liu, and Y.-G. Min, Journal of Alloys and Compounds p. 165559 (2022).
[108] J. Zhai, Z. Lei, K. Sun, and S. Zhu, Electrochimica Acta p. 140595 (2022).
[109] X. Li, Y. Tang, L. Liu, Y. Zhang, R. Sheng, and Y. NuLi, Journal of Colloid and Interface Science **608**, 2455 (2022).
[110] Z. Wang, X. Zheng, A. Chen, Y. Han, L. Wei, and J. Li, ACS Materials Letters **4**, 1436 (2022).
[111] Y. Du, B. Zhang, W. Zhang, H. Jin, J. Qin, J. Wan, Y. Zhang, Z. Wang, J. Zhang, and G. Chen, Journal of Alloys and Compounds **896**, 162901 (2022).
[112] J. Zhu, X. Zhang, H. Gao, Y. Shao, Y. Liu, Y. Zhu, J. Zhang, and L. Li, Journal of Power Sources **518**, 230731 (2022).
[113] Y. Feng, Y. Feng, Y. Zhang, L. Sun, X. Li, M. Meng, Y. Zhu, and K. Liu, Journal of Power Sources **545**, 231944 (2022).
[114] W. Lv, G. Wu, X. Li, J. Li, and Z. Li, Energy Storage Materials **46**, 138 (2022).
[115] H. Xu, R. Zheng, D. Du, L. Ren, R. Li, X. Wen, C. Zhao, and C. Shu, Applied Materials Today **27**, 101464 (2022).
[116] W. Du, L. Miao, Z. Song, X. Zheng, Y. Lv, D. Zhu, L. Gan, and M. Liu, Journal of Power Sources **536**, 231512 (2022).
[117] X. Zhao, Z. Zhang, H. Zhang, S. Xiong, X. Xu, X. Fan, and S. Wang, Journal of Alloys and Compounds **902**, 163702 (2022).
[118] J. Shi, Y. Hou, Z. Liu, Y. Zheng, L. Wen, J. Su, L. Li, N. Liu, Z. Zhang, and Y. Gao, Nano Energy **91**, 106651 (2022).
[119] G.-H. Dong, Y.-Q. Mao, Y.-Q. Li, P. Huang, and S.-Y. Fu, Electrochimica Acta **420**, 140464 (2022).
[120] J. Zhao, Y. Qi, Q. Yang, T. Huang, H. Wang, Y. Wang, Y. Niu, Y. Liu, S. Bao, and M. Xu, Chemical Engineering Journal **429**, 131997 (2022).
[121] P. Liang, T. Xu, K. Zhu, Y. Rao, H. Zheng, M. Wu, J. Chen, J. Liu, K. Yan, J. Wang, et al., Energy Storage Materials **50**, 63 (2022).
[122] Y. Yang, J. Chen, Q. Gao, Y. Feng, F. Xing, and M. Yao, Current Applied Physics **34**, 24 (2022).
[123] X. Li, X. Zhu, Z. Cao, Z. Xu, J. Shen, and M. Ye, Small **18**, 2105325 (2022).
[124] X. Huo, X. Wang, J. Li, B. Zhang, Y. Zhang, T. Qin, and F. Kang, Science China Materials **65**, 85 (2022).
[125] R. Pai, V. Natu, M. Sokol, M. Carey, T. Greszler, M. W. Barsoum, and V. Kalra, Materials Today Energy **27**, 101000 (2022).
[126] B. Anasori, M. R. Lukatskaya, and Y. Gogotsi, Nature Reviews Materials **2**, 1 (2017).
[127] J. Zhou, X. Zha, F. Y. Chen, Q. Ye, P. Eklund, S. Du, and Q. Huang, Angewandte Chemie International Edition **55**, 5008 (2016).
[128] M. Mirzaeian, Q. Abbas, M. R. Hunt, A. Galeyeva, and R. Raza, Advanced Functional Materials **23**, 947 (2021).
[129] B. Anasori and Y. Gogotsi, *2D Metal Carbides and Nitrides (MXenes)* (Springer, 2019).
[130] J. Chen, Q. Huang, H. Huang, L. Mao, M. Liu, X. Zhang, and Y. Wei, Nanoscale **12**, 3574 (2020).
[131] M.-Q. Zhao, C. E. Ren, M. Alhabeb, B. Anasori, M. W. Barsoum, and Y. Gogotsi, ACS Applied Energy Materials **2**, 1572 (2019).
[132] Z. Zhang, S. Dong, Z. Cui, A. Du, G. Li, and G. Cui, Small Methods **2**, 1800020 (2018).
[133] K. Zhu, C. Wang, Z. Chi, F. Ke, Y. Yang, A. Wang, W. Wang, and L. Miao, Frontiers in Energy Research **7**, 123 (2019).
[134] C. Wang, K. Su, W. Wan, H. Guo, H. Zhou, J. Chen, X. Zhang, and Y. Huang, Journal of Materials Chemistry A **2**, 5018 (2014).
[135] J. H. Lee, J. Kang, S.-W. Kim, W. Halim, M. W. Frey, and Y. L. Joo, ACS omega **3**, 16465 (2018).
[136] Y. Wang, T. Guo, E. Alhajji, Z. Tian, Z. Shi, Y.-Z. Zhang, and H. N. Alshareef, Advanced Energy Materials p. 2202860 (2022).
[137] H. T. Le, D. T. Ngo, P. N. Didwal, J. G. Fisher, C.-N. Park, I.-D. Kim, and C.-J. Park, Journal of Materials Chemistry A **7**, 3150 (2019).
[138] K. Wang, Y. Zhou, W. Xu, D. Huang, Z. Wang, and M. Hong, Ceramics International **42**, 8419 (2016).
[139] J. Michael, Z. Qifeng, and W. Danling, Nanomaterials

and Nanotechnology **9**, 1847980418824470 (2019).
[140] S. Seyedin, J. Zhang, K. A. S. Usman, S. Qin, A. M. Glushenkov, E. R. S. Yanza, R. T. Jones, and J. M. Razal, Global Challenges **3**, 1900037 (2019).